Decoupling Scheme for Virtual Synchronous Generator Controlled Wind Farms Participating in Inertial Response

Jiangbei Xi, Hua Geng, *Senior Member*, *IEEE*, and Xin Zou

***Abstract*—In this paper, the dynamic coupling between the wind turbine rotor speed recovery (WTRSR) and inertial response of the conventional virtual synchronous generator (VSG) controlled wind farms (WFs) is analyzed. Three distinguishing features are revealed. Firstly, the inertial response characteristics of VSG controlled WFs (VSG-WFs) are impaired by the dynamic coupling. Secondly, when the influence of WTRSR is dominant, the inertial response characteristics of VSG-WFs are even worse than the condition under which WFs do not participate in the response of grid frequency. Thirdly, this phenomenon cannot be eliminated by only enlarging the inertia parameter of VSG-WFs, because the influence of WTRSR would also increase with the enhancement of inertial response. A decoupling scheme to eliminate the negative influence is then proposed in this paper. By starting the WTRSR process after inertial response period, the dynamic coupling is eliminated and the inertial response characteristics of WFs are improved. Finally, the effectiveness of the analysis and the proposed scheme are verified by simulation results.**

***Index Terms*—Wind turbine rotor speed recovery (WTRSR), inertial response, virtual synchronous generator (VSG), decoupling scheme.**

I. Introduction

With the increase of wind power penetration in the power grid, the mechanical inertia of the entire system reduces, which results in an increasing rate of change of frequency (RoCoF) and a decrease of frequency nadir during the frequency events [1]. High RoCoF would trigger the protection and disconnection of the embedded generators from the grid network. It further leads to the acceleration of frequency drop [1]. Low frequency nadir leads to the decrease of under-frequency load-shedding margin [2], [3]. Therefore, in light of concerns associated with high penetration levels of the wind, inertial response from wind power is required by many power system operators (PSOs) [4].

The specific grid code requirements for inertial response from wind power vary according to different PSOs. In the case of a significant frequency deviation, wind turbines (WTs) are required to provide an active power response equivalent to that of a synchronous generator (SG) with an inertial constant of 3.5 s for a period of 10 s in Hydro Quebec [5]. The European Network of Transmission System Operators for Electricity (ENTSO-E) considers that individual transmission system operators (TSOs) shall have the right to require a wind power generation facility to deliver an equivalent performance to conventional generation [6]. In some applications, the quantification of equivalent inertia parameters is needed, which should be determined by both TSOs and the turbine manufacturers [5], [7]-[12].

To obtain inertial response from wind power, both the energy source and the control scheme should be considered [13]-[23]. Currently, most of the wind farms (WFs) are operating in the maximum power production to pursue the maximum economic benefit. And the kinetic energy (KE) of WT rotor is usually taken as energy source for inertial response [13]-[15]. For this application, a WT rotor speed recovery (WTRSR) process is expected since the WT must restore to its previous operation point after inertial response [13]-[15].

For the control scheme, there are mainly two categories of methods in the literature. One aims to release a certain amount of energy to the power grid during frequency response [3], [16], e.g., GE's WindINERTIA™ control. The other is to release the energy with the performance similar to conventional SG [17]-[20], e.g., the control scheme of virtual SG (VSG). The control scheme of VSG studied in this paper for the characteristics is similar to SG [17]-[19].

The previous studies have pointed out the phenomenon that the inertial response characteristics of WT are impaired by the dynamic of maximum power point tracking (MPPT) controller [15], [19]. But the mechanism is still not clear. For example, this phenomenon can be solved by increasing the value of inertia parameter. However, as analyzed and verified in this paper, it is not effective.

According to the analysis in this paper, the dynamic coupling has three distinctive characteristics. Firstly, due to this dynamic coupling, the inertial response characteristics for VSG controlled WFs (VSG-WFs) are always impaired. Secondly, when the influence of WTRSR is dominant, VSG-

Manuscript received: May 20, 2019; accepted: September 30, 2019. Date of CrossCheck: September 30, 2019. Date of online publication: Apirl 9, 2020.

This work was supported by Science and Technology Project of State Grid Corporation of China (No. 5102-201956300A-0-0-00).

J. Xi and H. Geng (corresponding author) are with the Department of Automation, Tsinghua University, Beijing, China (e-mail: xijiangbei@126.com; genghua@tsinghua.edu.cn).

X. Zou is with the State Grid Economic and Technological Research Institute Co. Ltd., Beijing, China (e-mail: zouxin@chinasperi.sgcc.com.cn).

DOI: 10.35833/MPCE.2019.000341

WFs are harmful to the grid frequency response. Thirdly, this phenomenon cannot be eliminated by only enlarging the inertia parameter of VSG-WFs with the enhancement of inertial response, and the influence of WTRSR also increases. A decoupling scheme to eliminate the negative influence is then proposed in this paper. The dynamic coupling is eliminated by starting the WTRSR process after inertial response and the inertial response characteristics for WFs would also be improved.

In this paper, the analysis and verification are based on the permanent magnet SG (PMSG) based WFs for its increasing popularity [24]-[27]. The remainder of this paper is organized as follows. In Section II, the frequency response of power grid with WFs is analyzed and verified. A decoupling scheme to eliminate the influence of WTRSR to the inertial response characteristics for PMSG-based WFs is proposed in Section III. In Section IV, the effectiveness of the proposed scheme is verified by the simulation results. Finally, the conclusions are drawn in Section V.

II. Frequency Response of Power Grid with WFs

A. Frequency Response of Conventional Power Grid

1) Frequency Response Processes

The typical frequency response processes of the conventional SG-based power grid with frequency drop includes the following two stages as demonstrated in Fig. 1 [28], where f_{nom} is the nominal grid frequency.

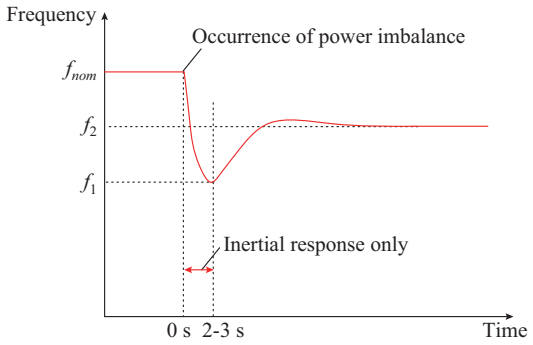

Fig. 1. Typical processes of frequency response.

1) Inertial response: when power disturbance occurs, SG would firstly respond automatically by changing its rotor speed, which is called inertial response with typical lasting time up to 2-9 s [17], [28]. Inertial response can support the grid frequency temporarily until primary frequency regulation starts.

2) Primary frequency regulation (PFR): PFR is implemented by the governor of SG with typical response time of several seconds. PFR can last from more than 10 s to several minutes based on the amount of reserved steam/water to provide additional continuous power.

2) Indexes of Frequency Response Performance

1) RoCoF: an index indicating how fast the frequency is changing.

2) Frequency nadir: the maximum frequency excursion before frequency starts to recover, i.e., f_1 in Fig. 1.

3) Settling frequency: the frequency when the PFR is stable, i.e., f_2 in Fig. 1.

B. Modeling of PMSG-based VSG-WFs

Figure 2 shows the equivalent model of power grid with large-scale WFs discussed in this paper. In Fig. 2, V_{dcref}, V_t, V_g are the reference value of DC bus voltage, WT terminal voltage and the grid voltage, respectively; P_{mppt}, P_{ref}, P_{L1}, P_{L2} are the MPPT value, the active power reference value of VSG, the active power of load L_1 and L_2, respectively; Q_{L1}, Q_{L2} are the reactive power of load L_1 and L_2, respectively; ω_{wt} is the rotor speed of WT; T_1, PCC, X_1 are the transformer, the point of common connection and line impedance, respectively.

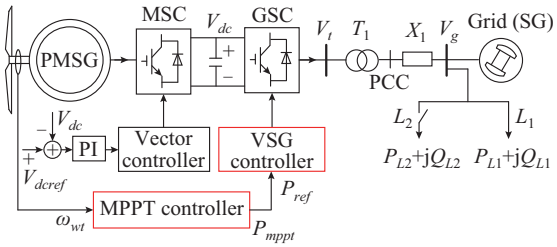

Fig. 2. Equivalent model of power grid with WFs.

The WFs are simply represented by a PMSG-based wind energy conversion system (WECS) for the study of frequency response. SG is used to emulate the power grid with reduced mechanical inertia. SG participates in both inertial response and PFR processes while WFs only participate in the inertial response. The load characteristics are simulated by two local loads L_1 and L_2. The VSG scheme is achieved by the grid-side converter (GSC). The DC bus voltage V_{dc} is controlled by the machine-side converter (MSC). Generally, the DC bus voltage control and the MPPT control are achieved by two different converters [27], [29]. Therefore, the MPPT control is achieved by GSC.

Because of the widely practical application, the power speed feedback (PSF) MPPT algorithm is studied in this paper [29]-[31]. The corresponding MPPT curve is shown in Fig. 3. The VSG scheme can be found in [21].

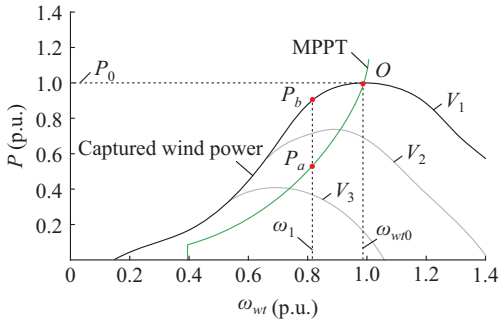

Fig. 3. Rotation speed characteristics of WT.

The active power control scheme of PMSG-based VSG-WFs can be expressed as follows. Equation (1) is the PSF MPPT algorithm, (2) is the VSG active power control algorithm and (3) shows the relationship between MPPT controller and VSG controller.

$$P_{mppt} = K_{mppt}\omega_{wt}^3 \tag{1}$$

$$P_{ref} - P_e = 2H_{vsg}\frac{\mathrm{d}\omega_{vsg}}{\mathrm{d}t} + D_{vsg}\left(\omega_{vsg} - \omega_{pcc}\right) \tag{2}$$

$$P_{ref} = P_{mppt} \tag{3}$$

where K_{mppt} is the coefficient related to WT characteristics; ω_{wt} is the WT rotor speed; P_{ref}, P_e, and ω_{vsg} are the input power, output power and virtual rotor frequency of VSG, respectively; ω_{pcc} is the frequency at PCC; and H_{vsg} and D_{vsg} are the virtual inertia constant and damping coefficient of VSG, respectively.

The reactive power control scheme of PMSG-based VSG-WFs is given as follows [21]:

$$V_1 = V_s - D_q Q_e \tag{4}$$

$$V_2 = \frac{K_Q\left(Q_{ref} - Q_e\right)}{s} \tag{5}$$

$$V_{vsg} = V_1 + V_2 \tag{6}$$

where V_s is the reference voltage value; D_q is the voltage droop constant; Q_e is the practical value of reactive power; K_Q is the integrator gain; Q_{ref} is the reference value of reactive power; and V_{vsg} is the terminal voltage of VSG. Because this paper is focused on frequency response, Q_{ref} is assumed to be 0.

C. Coupling Between WTRSR and Inertial Response of VSG-WFs

According to the power conservation of WT, we can obtain:

$$P_{capture} + P_{WTKE} = P_{mppt} + P_{IR} \tag{7}$$

where $P_{capture}$ is the captured wind power of WT, and according to Fig. 3, $P_{capture}$ varies with the WT rotor speed; P_{WTKE} is the power released from KE of WT rotor, and the two items are the power provided by WT; and P_{IR} is the power for inertial response. P_{IR} and P_{mppt} are the power released by WT. According to (2), P_{IR} can be expressed as:

$$P_{IR} = 2H_{vsg}\left(-\frac{\mathrm{d}\omega_{vsg}}{\mathrm{d}t}\right) + D_{vsg}\left[-\left(\omega_{vsg} - \omega_{pcc}\right)\right] \tag{8}$$

Taking the wind speed equals V_1 as an example. The stable operation point is point O in Fig. 3. Under this condition, both P_{mppt} and $P_{capture}$ are equal to P_0. And the rotor speed of WT is ω_{wt0}. When grid frequency drop event occurs, the KE of WT rotor should be released to support the grid frequency. Then the rotor speed of WT decreases. Taking the condition where the rotor speed of WT decreases from ω_{wt0} to ω_1 as an example, the corresponding P_{mppt} value is P_a, and $P_{capture}$ value is P_b. According to Fig. 3, $P_{mppt}(P_a)$ is smaller than $P_{capture}(P_b)$, and their differences will result in WTRSR. The corresponding power for WTRSR P_{WTRSR} is calculated as:

$$P_{WTRSR} = P_{capture} - P_{mppt} \tag{9}$$

By substituting (8) and (9) into (7), the power released from KE of WT rotor P_{WTKE} can be expressed as:

$$P_{WTKE} = P_{IR} - P_{WTRSR} \tag{10}$$

According to (10), the inertial response of VSG-WFs is always impaired by WTRSR because P_{WTKE} is negatively correlated with P_{WTRSR}.

Specifically, P_{WTRSR} increases with the release of KE of WT rotor. Therefore, at the beginning of the frequency drop event, the release of KE of WT rotor is small and the influence of P_{WTRSR} is not prominent. With the continuation of the frequency response process, the release of KE of WT rotor increases gradually and the influence of P_{WTRSR} becomes greater. When P_{IR} is smaller than P_{WTRSR}, WT absorbs energy from the power grid. Under this condition, the influence of WTRSR is dominant, and the inertial response characteristics of VSG-WFs are even worse than the condition where WFs do not participate in frequency response.

Particularly, this phenomenon cannot be eliminated by only enlarging the inertia parameter of VSG-WFs. With the enhancement of inertial response, more KE of WT rotor is released and in turn, the influence of WTRSR increases.

When the grid frequency increases, similar coupling and phenomenon can be observed.

D. Verification of Influence of WTRSR to Inertial Response

The model shown in Fig. 2 is adopted in the simulations. The power base is 1.5 MVA and the frequency base is 50 Hz. The parameters of WFs can be found in [27]. The rated power of SG and PMSG based WFs are 1.33 p.u. and 1.00 p. u., respectively. The grid regulates the frequency by its governor with permanent droop coefficient (4%). The inertia time constants of both grid and VSG-WFs are 4 s. The damping coefficient of VSG-WFs is chosen as 20 according to [21]. P_{L1} and P_{L2} are 1.63 p.u. and 0.82 p.u., respectively. The wind speed is 9 m/s. WFs operate at the maximum power point when t = 0 s and the load L_2 is switched on when t = 2 s.

Figure 4 shows the corresponding simulation results. In order to evaluate the frequency characteristics of VSG-WFs, the following two conditions are considered:

1) WFs are controlled by the original vector control (WFs-VC). In this application, the VSG controller in Fig. 2 is substituted by vector controller, and the output power of the WFs does not change with the frequency of the power grid.

2) WFs are replaced by an SG with the same capacity. This SG is different from the one which simulates the power grid with reduced mechanical inertia (noted as SG_{grid}) and participates in inertial response only.

In Fig. 4(a), (b) and (c), $H_{vsg} = 4$ s. The operation of VSG-WFs is analyzed as follows. At the beginning of frequency response processes (stage *a*), the inertial response plays a dominant role. The RoCoF of VSG-WFs shown in Fig. 4(c) is similar to SG and smaller than WFs-VC. In this stage, the influence of the coupling is invisible. After a period of time, the role of the WTRSR gradually emerges (stage *b*) and the frequency response performance (RoCoF and frequency nadir) of VSG-WFs is not as good as SG. With the continuation of frequency response, WTRSR then plays a dominant role (stage *c*). In this stage, both RoCoF and frequency nadir of VSG-WFs are the worst.

According to these simulation results, the original VSG-WFs can improve RoCoF, but worsen the frequency nadir.

Besides, as the results shown in Fig. 4(d), the larger H_{vsg} parameter, the smaller RoCoF, and the lower frequency nadir. The information of the virtual rotor frequency of VSG is shown in Fig. 5, where the same conclusions can also be obtained.

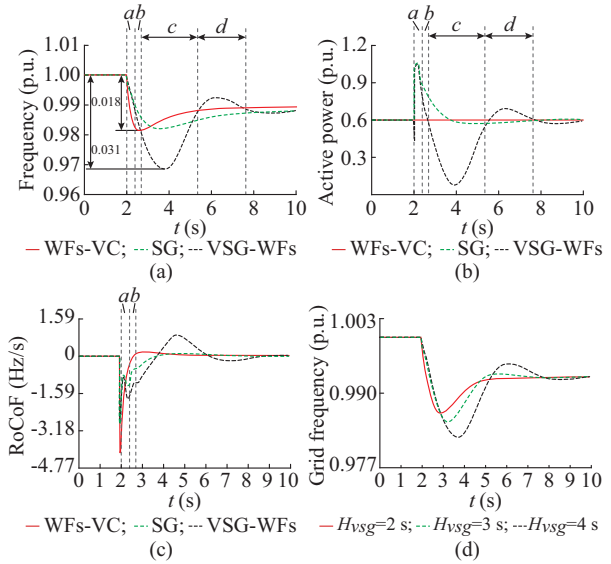

Fig. 4. Operation curves under different conditions. (a) Frequency response curves. (b) Output active power. (c) RoCoF curves. (d) Grid frequency comparison of different H_{vsg}.

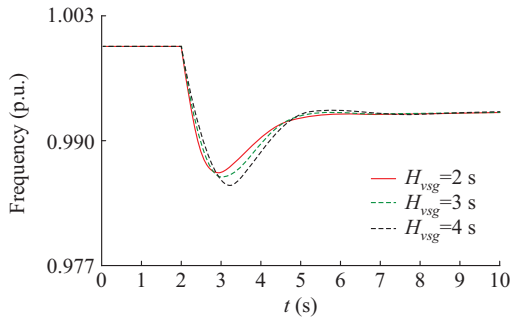

Fig. 5. Virtual rotor frequency of VSG under different conditions.

Therefore, the weakening of inertial response by WTRSR can not be offset by enhancing the effect of inertial response and a scheme to decouple WTRSR, and the inertial response in VSG-WFs should be proposed.

III Decoupling Scheme for VSG-WFs to Participate in Inertial Response

A. Scheme for Grid Frequency Drop Event

Figure 6 is the control diagram of the proposed decoupling scheme for VSG-WFs. Figure 7 shows the active power reference curves (APRC) of the proposed scheme.

In order to ensure the normal operation of WT, a minimum acceptable WT rotor speed ω_{wt} curve is defined ($F \rightarrow B$ curve in Fig. 7). The power at point F is equal to P_0 and the corresponding rotor speed is $\mu\omega_{wt0}$, where μ is the minimum rotor speed coefficient, e.g., $\mu = 0.9$ means the minimum acceptable WT rotor speed is 90% of the optimal rotor speed.

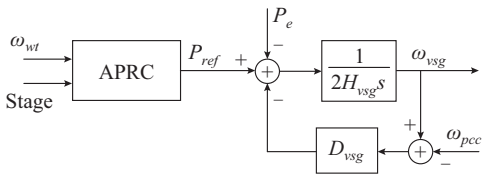

Fig. 6. Proposed scheme for VSG applied in WFs.

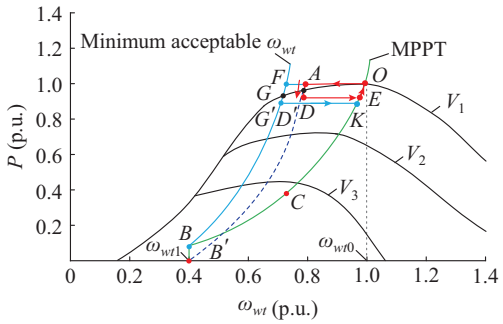

Fig. 7. APRC of proposed scheme when grid frequency decreases.

And the expression of $F \rightarrow B$ curve is obtained as follows:

$$P_{\omega\min}(\omega_{wt}) = \frac{K_{mppt}}{\mu^3}\omega_{wt}^3 \tag{11}$$

The flowchart of the proposed scheme is shown in Fig. 8. The detailed operation processes are as follows.

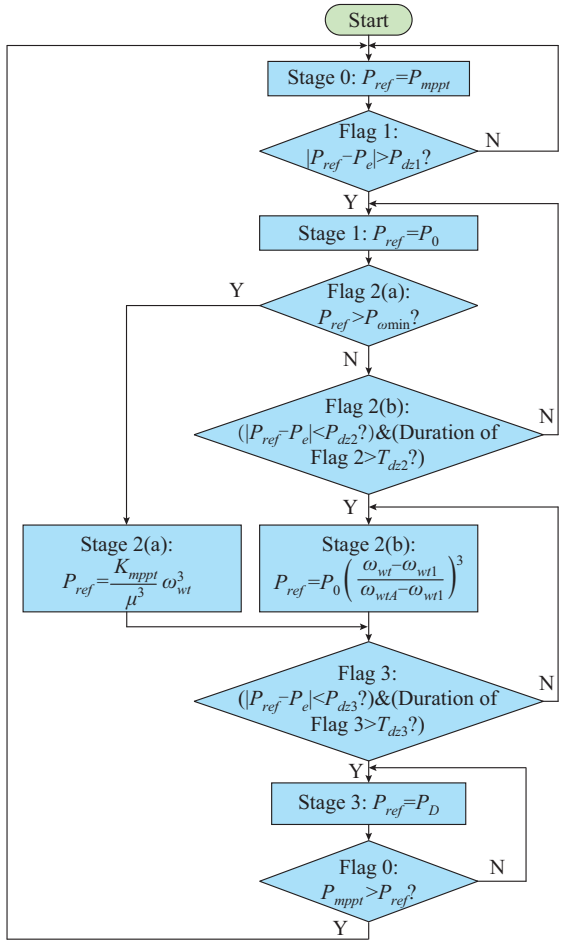

Fig. 8. Flowchart of proposed scheme.

1) Stage 0: Operation Stage of VSG-WFs, B→O Curve

In this stage, the original VSG scheme is employed to control the WT. The wind speed is assumed to be V_1. Point O is the corresponding optimal operation point and the steady-state operation point of VSG-WFs. The corresponding optimal power is P_0 and the WT rotor speed is ω_{wt}.

When the grid frequency drop event occurs, VSG-WFs start the inertial response automatically. If the power imbalance is small, the influence of WTRSR is not significant and the WFs can still operate with the original VSG scheme. If the disturbance is large enough, the influence of WTRSR on inertial response cannot be ignored any more, and then the dynamic of WTRSR should be decoupled with that of inertial response. Therefore, the flag to leave this stage can be chosen as $|P_0 - P_e| > P_{dz1}$ (Flag 1).

2) Stage 1: Disabled Stage of MPPT Operation, O→F Curve

When Flag 1 is obtained, the decoupling scheme is activated. It will disable the MPPT operation during inertial response stage and P_{ref} is maintained at P_0.

3) Stage 2: Approximately Optimal Power Operation Stage

After inertial response period, WTRSR should be realized. Based on whether the WT rotor speed is reduced to the minimum value during inertia response stage, the operation can be divided into two specific conditions:

1) Stage 2(a) represents the minimum rotor speed during the operation, $F\rightarrow G$ curve: according to (11), when the WT rotor speed is decreased to be smaller than the minimum acceptable WT rotor speed $\mu\omega_{wt0}$, $P_{\omega,\min} < P_0$ is obtained. Thereafter, the grid frequency is supported by SGs in the power grid and the operation goal of WT is to maintain the stable operation without large power disturbance to the power grid. In the proposed scheme, this goal is achieved by setting the reference of the VSG controller according to the minimum rotor speed $F\rightarrow B$ curve. And P_{ref} is obtained according to (11). Because the reference of the proposed scheme is the output power, the small-signal stability caused by the mismatch between the expected output power and the practical output power [28] would not happen. When the system is stable, WFs will stay at point G and the corresponding captured wind power is P_G. In this stage, the grid frequency is mainly supported by the PFR of SG. Therefore, the influence of the WT output power which decreases from P_0 to P_G is small.

2) Stage 2(b) represents the maximum available power operation, $A\rightarrow D$ curve: if the KE of WT rotor is enough, the WT rotor speed will not reach the minimum value when the inertial response finishes. After PFR of the grid is built, the power imbalance is mainly undertaken by the grid. WFs gradually operate into its steady state. Therefore, the flag of this stage can be chosen as $|P_{ref} - P_e| < P_{dz2}$ (Flag 2(b)). To make sure that the judgment of operation stage is correct, the duration of Flag 2(b) should last at least T_{dz2}.

Assume that the operation point is point A in Fig. 8 when Flag 2(b) is obtained. Then WFs can operate following $A\rightarrow B'$ curve to its maximum available power. The expression is:

$$P_{ref}(\omega_{wt}) = P_0\left(\frac{\omega_{wt}-\omega_{wt1}}{\omega_{wt,A}-\omega_{wt1}}\right)^3 \tag{12}$$

where $\omega_{wt,A}$ is the rotor speed of point A; and ω_{wt1} is the WT cut in rotor speed (point B' in Fig. 10). WFs will stays at point D when the system is stable and the corresponding captured wind power P_D is larger than P_G.

The operation after Stage 2 for the two conditions is similar and Stage 2(b) is taken as an example to illustrate the basic principles.

4) Stage 3: WTRSR Stage, D→D'→E Curve

When the grid frequency is stable, WFs operate stably and the input and output power of VSG are nearly the same. Then $|P_{ref} - P_e| < P_{dz3}$ (Flag 3) is obtained. To make sure that the judgment of operation stage is correct, the duration of Flag 3 is required to be at least T_{dz3}. Then the WT rotor speed can start to recover.

In order to achieve WTRSR smoothly, P_{ref} is controlled to equal $P_{D'}$ which is a little bit smaller than P_D, e.g., 99%×P_D. Then the WT rotor speed and the corresponding MPPT value increase. When $P_{mppt} > P_{D'}$ (Flag 0) is obtained, WFs can switch to VSG-WFs operation automatically.

5) Stage 0: VSG-WF Operation Stage, E→O Curve

In this stage, WFs are controlled to operate at the optimal power point O by MPPT control scheme.

The operation path of the proposed scheme is $O\rightarrow A\rightarrow D\rightarrow D'\rightarrow E\rightarrow O$ or $O\rightarrow F\rightarrow G\rightarrow G'\rightarrow K\rightarrow O$.

B. Scheme for Event of Grid Frequency Increase

For practical operation, the grid frequency increase should be considered. The corresponding decoupling scheme is similar to the above situation of grid frequency decrease. The operation curves are shown in Fig. 9. $A_1\rightarrow D_1$ is the maximum ω_{wt} curve, the expression is the same to (11) with a coefficient μ larger than 1, e.g., $\mu = 1.1$.

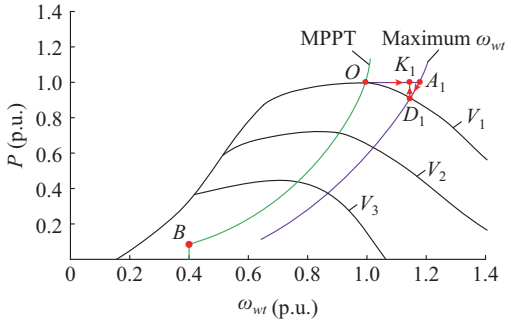

Fig. 9. APRC of proposed scheme when grid frequency increases.

The operation stages corresponding to this condition are described as follows. WFs originally operate in VSG-WFs operation stage (Stage 0, $O\rightarrow B$ curve). When Flag 1 is satisfied, WFs operate in inertial response stage, and the MPPT operation is disabled (Stage 1, $O\rightarrow A_1$ curve). The WT rotor speed increases until the value reaches to the maximum WT rotor speed, then WFs operate in approximately optimal power operation stage (Stage 2, $A_1\rightarrow D_1$ curve). When Flag 3 is satisfied, WFs operate in WTRSR stage (Stage 3, curve $D_1K_1\rightarrow K_1O$). The WT rotor speed decreases until the value reaches to the optimal rotor speed. Then the WFs operate in VSG-WF operation stage again (Stage 0, $O\rightarrow B$ curve). The operation path is $O\rightarrow A_1\rightarrow D_1\rightarrow K_1\rightarrow O$.

C. Design of Control Parameters

1) Design of μ

μ is the parameter to define the minimum or maximum WT rotor speed curve. Because the design of the two conditions is similar, we take the condition for the curve of the minimum WT rotor speed as an example. In fact, μ is determined by the requirements for the stored energy for inertial response and the captured wind power.

2) Stored Energy for Inertial Response

The stored energy for inertial response is the KE of WT rotor between the MPPT point and the minimum rotor speed point ΔE_{KE}. The expression is given as:

$$\Delta E_{KE} = \frac{1}{2} J_{wt} \omega_{wt0}^2 - \frac{1}{2} J_{wt} \omega_{wt,\min}^2 = \frac{1}{2} J_{wt} \omega_{wt0}^2 \left(1-\mu^2\right) \quad (13)$$

where J_{wt} is the inertia of the wind turbine; ω_{wt0} and $\omega_{wt,\min}$ are the nominal WT rotor speed and the minimum WT rotor speed, respectively.

The stored KE of WT rotor is released to the power grid by inertial response of VSG, and the maximum energy released by the VSG ΔE_{IR} is expressed as:

$$\Delta E_{IR} = \frac{1}{2} J_{vsg} \omega_{vsg0}^2 - \frac{1}{2} J_{vsg} \omega_{\min}^2 \quad (14)$$

where J_{wt} is the virtual inertia of the VSG; ω_{vsg0} is the nominal grid angular frequency; and $\omega_{\min}$ is the minimum grid angular frequency defined by grid code.

The energy released by the VSG should be smaller than the stored energy. Then according to (13) and (14), the following expression is obtained:

$$J_{vsg} \le J_{wt} \frac{\omega_{wt0}^2 \left(1-\mu^2\right)}{\omega_{vsg0}^2 - \omega_{\min}^2} \quad (15)$$

Because the rated power of WT and VSG is the same, the expression for inertia constant is also obtained:

$$H_{vsg} \le H_{wt} \frac{\omega_{vsg0}^2}{\omega_{vsg0}^2 - \omega_{\min}^2} \left(1-\mu^2\right) \quad (16)$$

3) Captured Wind Power

The relationship between the WT captured wind power and the WT rotor speed is given as follows [24]:

$$P_{wt} = K_{wt} C_p \quad (17)$$

$$C_p \approx 0.0059\lambda + 0.645\left(\frac{116}{\lambda+0.2} - 6\right) \mathrm{e}^{-21\left(\frac{1}{\lambda+0.2}\right)} \quad (18)$$

$$\lambda = K_\lambda \omega_{wt} \quad (19)$$

where C_p is the power coefficient; λ is the tip-speed ratio; and K_{wt} and K_λ are the coefficients related to the characteristics of WT. For practical operation, the deviation of the WT captured wind power from the optimal power is required to be as small as possible.

The inertia constant of WT is 4.32 s [27]. Generally, the inertia constant of VSG is required to no smaller than 4 s. According to (16), if the nominal grid frequency is 50 Hz and the minimum grid frequency is 48 Hz, the value of μ should be smaller than 0.963. According to (17)-(19), when μ equals to 0.9, the captured power of this point is larger than 97%×P_{mppt} at the rated wind speed (11 m/s).

4) Design of P_{dz1}

To estimate the influence of WTRSR to inertial response, the equivalent inertia constant and damping coefficient are deduced.

As mentioned above, the coupling is introduced by the operation of MPPT controller. Therefore, the equivalent parameters are obtained by comparing with the condition where MPPT controller is disabled in the inertial response stage. Under this condition, the input power of VSG equals to the optimal power P_0 according to Fig. 3. And the corresponding swing equation can be expressed as:

$$P_0 - P_e = 2H_{eq} \frac{\mathrm{d}\omega_{vsg}}{\mathrm{d}t} + D_{eq}\left(\omega_{vsg} - \omega_{pcc}\right) \quad (20)$$

By comparing (13) with (2), the equivalent parameters H_{eq} and D_{eq} can be obtained as:

$$\eta = \frac{H_{eq}}{H_{vsg}} = \frac{D_{eq}}{D_{vsg}} = \frac{P_0 - P_e}{P_{ref} - P_e} \quad (21)$$

where η is the coefficient between the equivalent parameters and their corresponding setting parameters.

The smallest acceptable equivalent inertia is marked as $\eta_{\min} H_{vsg}$. When $H_{eq} > \eta_{\min} H_{vsg}$, the influence of WTRSR on inertial response can be ignored. Otherwise, the decoupling scheme proposed in this paper should be activated. According to (1), (3) and (21), the minimum H_{eq} is obtained when the WT rotor speed reaches the minimum acceptable value $\mu\omega_{wt0}$. Therefore, the decoupling scheme would be activated when $H_{eq}\left(\mu\omega_{wt0}\right) \le \eta_{\min} H_{vsg}$ and the corresponding relationship is:

$$H_{eq}\left(\mu\omega_{wt0}\right) = \left(1 - \frac{P_0 - K_{mppt}\left(\mu\omega_{wt0}\right)^3}{P_e - K_{mppt}\left(\mu\omega_{wt0}\right)^3}\right) H_{vsg} \le \eta H_{vsg,\min} \quad (22)$$

Considering $P_0 = K_{mppt}\omega_{wt0}^3$, P_{dz1} is obtained as:

$$P_{dz1} = \left|P_0 - P_e\right| = P_0\left(1-\mu^3\right)\frac{1}{\eta_{\min}} \quad (23)$$

When μ = 0.9 and $\eta_{\min}$ = 0.85, the value of P_{dz1} is 5%P_0.

5) Design of P_{dz2}, T_{dz2}, P_{dz3}, T_{dz3}

P_{dz2} and T_{dz2} are parameters used to estimate the start of PFR of SG in the power grid. In this stage, the disturbance of the power grid is mainly undertaken by SG, and P_{IR} of WT is small. Therefore, the value of P_{dz2} should be small, e.g., $1\% \times P_0$. T_{dz2} is the period of Flag 2(b). To make sure the judgment of the operation stage is correct, the larger T_{dz2} is the better. Considering the regulation time of PFR, T_{dz2} is recommended to be no more than 1 s. P_{dz3} and T_{dz3} are parameters used to estimate that the grid frequency is stable. The power difference between P_{ref} and P_e in this stage is nearly equal to 0. Therefore, the P_{dz3} value should be very small, e.g., $0.2\% \times P_0$. T_{dz3} is the period of Flag 3. To make sure the judgment of the operation stage is correct, the larger T_{dz3} is better. Because the next stage is the WTRSR stage, a shorter T_{dz3} means that WT can operate in MPPT mode more quickly. Then, more power production can be obtained. In this paper, T_{dz3} is also recommended to be no more than 1 s.

IV Simulation Studies

The theoretical analysis and the proposed scheme are verified based on MATLAB 2014a/Simulink platform. The model study has already shown in Fig. 2. The grid is represented by a 2 MVA SG, the PMSG-based WF is rated at 1.5 MVA and the capacity of wind power penetration is around 42.9%. The power grid regulates the frequency by its governor with permanent droop coefficient 4%. The parameters of WFs can be found in [27]. The inertia time constant of both grid and VSG-WFs is 4 s. The damping coefficient of VSG-WFs is chosen as 20 according to [21]. The power base is 1.5 MVA and the frequency base is 50 Hz in the simulation results. $P_{dz1}=5\%\times P_0$, $P_{dz2}=1\%\times P_0$, $P_{dz3}=0.2\%\times P_0$, $T_{dz2}=50$ ms and T_{dz3} = 500 ms. In addition to VSG-WFs and the proposed scheme, the simulation studies of WFs-VC and WFs substituted by an SG with the same capacity are carried out. The minimum rotor speed coefficient is 0.9 and the maximum rotor speed coefficient is 1.1.

A. Verification in Equivalent Model of Power Grid with WFs

1) Performance When WT Rotor Speed is not Reduced to Minimum Value

P_{L1} and P_{L2} are set to be 1.63 p.u. and 0.2 p.u., respectively. The wind speed is 9 m/s. The load L_2 is switched on when t = 5 s. The effectiveness of the judgment of the stage signals is verified in Fig. 10. Figure 10(a) shows the results during frequency response. The initial stage is VSG-WFs operation stage (Stage 0). When a power disturbance occurs, the flag $|P_{ref}-P_e|>P_{dz1}$ is obtained for the difference between P_{ref} and P_e. The operation enters MPPT operation disabled stage (Stage 1). When PFR of the grid is built, the power imbalance of the system is mainly supported by PFR of SG in the grid. $|P_{ref}-P_e|<P_{dz2}$ is obtained. After waiting T_{dz2}, the operation enters Stage 2(b). WFs operate steadily. When $|P_{ref}-P_e|<P_{dz3}$ and after waiting T_{dz3}, WFs enter WTRSR stage (Stage 3). In WTRSR stage, WT rotor speed increases and the value of MPPT increases, too. If $P_{mppt}>P_{ref}$, WFs can switch to VSG-WFs operation stage (Stage 0) automatically. Figure 10(b) shows the results during MPPT operation. The wind speed increases to 9.5 m/s when $t_1=20$ s and decreases to 9 m/s when $t_2=28$ s. According to Fig. 10(b), the difference between P_{ref} and P_e is very small during MPPT operation. And WFs keeps in VSG-WFs operation stage (Stage 0).

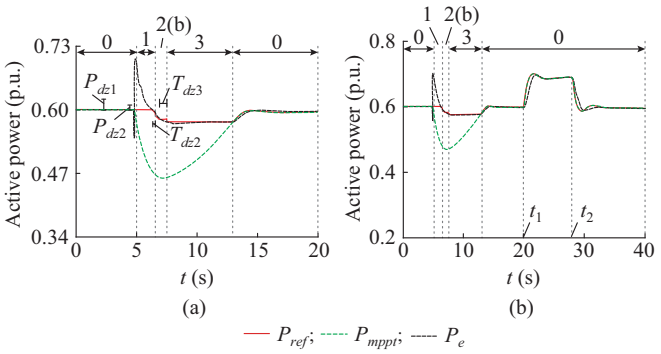

Fig. 10. Operation stage signals of proposed scheme. (a) During frequency response. (b) During MPPT operation.

Figure 11 shows the results for factors considered in frequency response. Figure 11(a) presents the curves of grid frequency response. The frequency support capability of the proposed scheme is the same as SG during inertial response stage (Stage 1), which means the coupling between WTRSR and inertial response is eliminated. After inertial response stage, the WTRSR control is activated. The frequency nadir of the proposed scheme is better than VSG-WFs with 0.0015 p. u. (0.075 Hz) improved. Figure 11(b) shows the RoCoF curves under different conditions. Compared to VSG-WFs, the maximum RoCoF with the proposed scheme is decreased with 0.065 Hz/s.

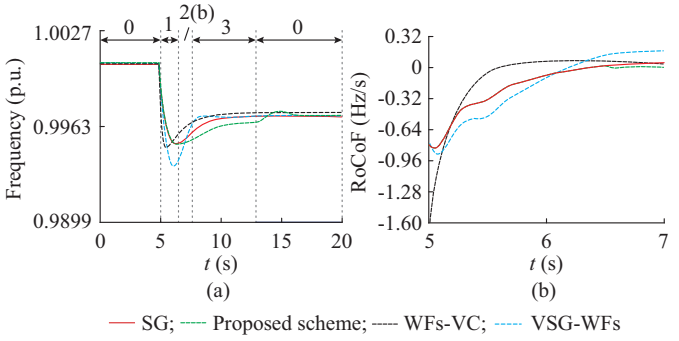

Fig. 11. Results for factors considered in frequency response. (a) Grid frequency response. (b) RoCoF curves.

Figure 12 shows the WFs operation curves under different conditions. Figure 12(a) presents the active power. For the proposed scheme, during inertial response stage (Stage 1), P_{ref} is constant and the influence of WTRSR is eliminated. The output power equals to that of SG. During Stage 2(b) and Stage 3, due to the WTRSR operation, the output power of decoupling control is a bit smaller than that of SG. For VSG-WFs, the output power of VSG-WFs is the smallest in inertial response stage. This means that its frequency support performance is the worst. Figure 12(b) presents the curves of WT rotor speed. Compared to VSG-WFs, the decrease of the WT rotor speed of the proposed scheme is larger, which means the proposed scheme can release more energy to the power grid. The recovery process of the proposed scheme is longer because inertial response and WTRSR are decoupled.

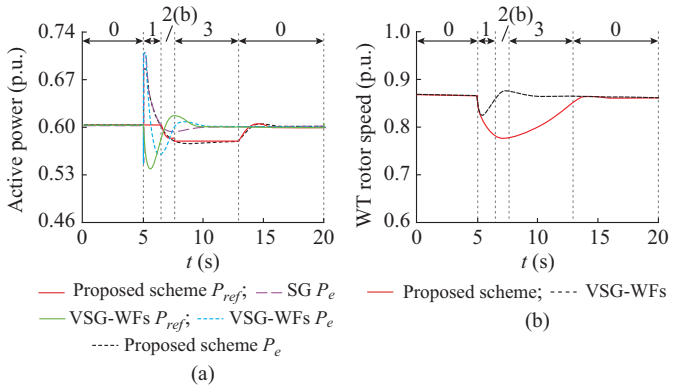

Fig. 12. WT operation curves under different conditions. (a) Output active power. (b) WT rotor speed curves.

The frequency nadir improvement of the proposed scheme

ξ is given as:

$$\xi = \Delta f_{VSG} - \Delta f_{PS} \tag{24}$$

$$\Delta f = f_{nom} - f_1 \tag{25}$$

where f_{VSG} and f_{PS} are the maximum grid frequeny drop of the original VSG scheme and the proposed scheme, respectively. The maximum grid frequeny drop Δf is calculated according to (25). f_{nom} and f_1 are defined according to Fig. 1. Figure 13 shows the corresponding results with different wind speeds. The results verify that the proposed scheme is robost with different wind speeds.

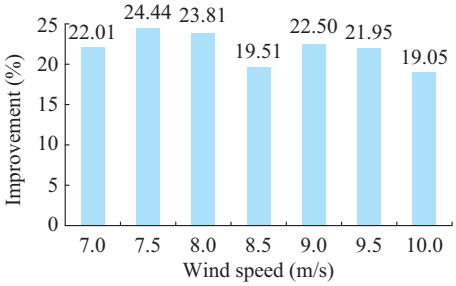

Fig. 13. Frequency nadir improvement of proposed scheme under different wind speeds.

2) Performance When WT Rotor Speed Reaches Minimum Value

P_{L1} and P_{L2} are set as 1.63 p.u. and 0.13 p.u., respectively. The initial wind speed is 9 m/s. L_2 is switched on when $t = 5$ s. To emulate the condition when KE of WT rotor is insufficient and the WT rotor speed is reduced to the minimum value in inertial response stage, the wind speed is decreased to 8 m/s when $t = 5$ s and back to 9 m/s when $t = 6$ s.

Figure 14(a) presents that the operation enters Stage 2(a) when the value of MPPT is smaller than the acceptable minimum value. The other operation stages are similar to the condition where WT rotor speed is not reduced to the minimum value. Figure 14(b) presents the frequency response curves. The frequency drop of the proposed scheme is much smaller than that of VSG-WFs, which is about 0.0013 p.u. (0.065 Hz). Figure 14(c) presents the curves of WT rotor speed. Compared to VSG-WFs, the decrease of the WT rotor speed of the proposed scheme is larger, which means the proposed scheme can release more energy to the power grid.

B. Verification in IEEE 4-machine 2-area System

The benchmark IEEE 4-machine 2-area system for power system study is carried out to verify the effectiveness of the proposed scheme. The simulation model is shown in Fig. 15.

The parameters of the IEEE 4-machine 2-area system can be found in [28]. The SG1 in [28] is substituted by a PMSG-based WF with the same capacity. The wind power penetration is around 24% in this system. $P_0 : P_7 : P_9 = 2 : 3 : 4$. To emulate the condition of grid frequency drop, L_0 is switched on when $t = 1$ s and the corresponding frequency response curves are shown in Fig. 16(a). To emulate the condition of grid frequency increase, L_0 is switched on before the system is stable and is switched off when $t = 1$ s. The corresponding frequency response curves are shown in Fig. 16(b).

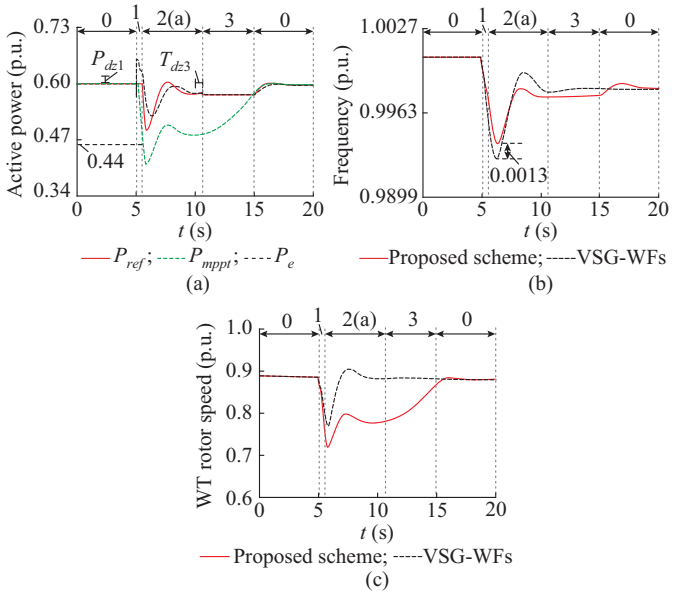

Fig. 14. WT operation curves in this case. (a) Output active power. (b) Grid frequency response. (c) WT rotor speed.

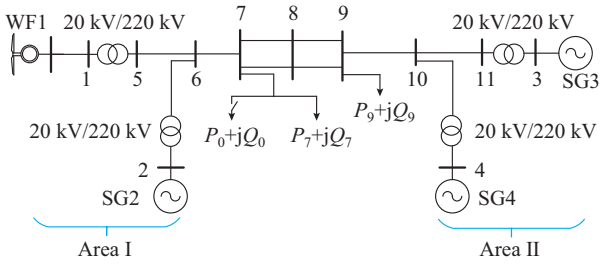

Fig. 15. Simulation model of IEEE 4-machine 2-area system.

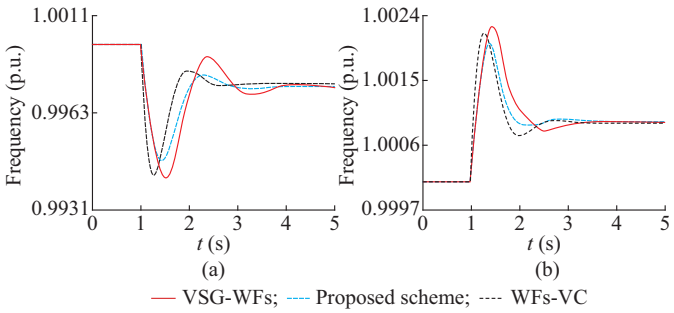

Fig. 16. Simulation results in IEEE 4-machine 2-area system. (a) Frequency drop event occurs. (b) Frequency increase event occurs.

According to the results shown in Fig. 16, the frequency response in both frequency drop condition and frequency increase condition of the proposed scheme are better than VSG-WFs during inertial response.

V. Conclusion

In this paper, a decoupling scheme is proposed to eliminate the coupling between WTRSR and inertial response in conventional VSG-WFs. By adopting the proposed scheme, the negative influence of WTRSR on the inertial response characteristic of VSG-WFs is eliminated. The inertial re-

sponse characteristics of WFs are improved. The analysis on the coupling and the proposed scheme is verified by the simulation results. In future study, the proposed scheme can be applied to doubly-fed induction generator (DFIG) based WFs and inertial emulation schemes of df/dt type. More work should be done for the application under the conditions of unbalanced grid voltage.

REFERENCES

[1] S. Kuenzel, L. P. Kunjumuhammed, B. C. Pal *et al*., "Impact of wakes on wind farm inertial response," *IEEE Transactions on Sustainable Energy*, vol. 5, no. 1, pp. 237-245, Jan. 2014.

[2] N. Miller, M. Shao, and S. Venataraman. (2019, Nov.) California ISO: frequency response study. [Online]. Available: http://www.uwig.org/Report-FrequencyResponseStudy.pdf

[3] E. Muljadi, V. Gevorgian, M. Singh *et al*., "Understanding inertial and frequency response of wind power plants," in *Proceedings of 2012 IEEE Power Electronics and Machines in Wind Applications*, Denver, USA, Jul. 2012, pp. 1-8.

[4] C. Jauch, J. Matevosvan, T. Ackermann *et al*., "International comparison of requirements for connection of wind turbines to power systems," *Wind Energy*, vol. 8, no. 3, pp. 295-306, Jul. 2005.

[5] J. Brisebois and N. Aubut, "Wind farm inertia emulation to fulfill Hydro-Québec's specific need," in *Proceedings of 2011 IEEE PES General Meeting*, Detroit, USA, Jul. 2011, pp. 1-7.

[6] EirGrid and SONI, "Ensuring a secure, reliable and efficient power system in a changing environment," Technic Report, 2011.

[7] S. Wachtel and A. Beekmann, "Contribution of wind energy converters with inertia emulation to frequency control and frequency stability in power systems", in *Proceedings of 8th International Workshop on Large-scale Integration of Wind Power and on Transmission Networks for Offshore Wind Farms*, 2009.

[8] M. Dernbach, D. Bagusche, and S. Schrader, "Frequency control in Québec with DFIG wind turbines," in *Proceedings of 9th International Workshop on Large-scale Integration of Wind Power and on Transmission Networks for Offshore Wind Farms*, San Diego, USA, Jul. 2012, pp. 20-26.

[9] M. Fecteau, C-E. Langlois, J. Marques *et al*., "Assessment of ENERCON WEC grid performance based on Hydro-Québec system requirements: a cooperation between ENERCON and Hydro-Québec," in *Proceedings of 9th International Workshop on Large-scale Integration of Wind Power and on Transmission Networks for Offshore Wind Farms*, San Diego, USA, Jul. 2012, pp. 1-8.

[10] L. Ruttledge, N. W. Miller, J. O'Sullivan *et al*., "Frequency response of power systems with variable speed wind turbines," *IEEE Transactions on Sustainable Energy*, vol. 3, no. 4, pp. 683-691, Oct. 2012.

[11] ENTSO-E, "Draft Requirements for Grid Connection Applicable to all Generators," Technic Report, 2011.

[12] L. Ruttledge and D. Flynn, "System-wide inertial response from fixed speed and variable speed wind turbines," in *Proceedings of 2011 IEEE PES General Meeting*, Detroit, USA, Jul. 2011, pp. 1-7.

[13] L. Ruttledge and D. Flynn, "Emulated inertial response from wind turbines: gain scheduling and resource coordination," *IEEE Transactions on Power Systems*, vol. 31, no. 5, pp. 3747-3755, Sept. 2016.

[14] F. Liu, Z. Liu, S. Mei *et al*., "ESO-based inertia emulation and rotor speed recovery control for DFIGs," *IEEE Transactions on Energy Conversion*, vol. 32, no. 3, pp. 1209-1219, Sept. 2017.

[15] Y. Wang, J. Meng, X. Zhang *et al*., "Control of PMSG-based wind turbines for system inertial response and power oscillation damping," *IEEE Transactions on Sustainable Energy*, vol. 6, no. 2, pp. 565-574, Apr. 2015.

[16] N. W. Miller, K. Clark, and M. Shao, "Frequency responsive wind plant controls: impacts on grid performance," in *Proceedings of 2011 IEEE PES General Meeting*, Detroit, USA, Jul. 2011, pp. 1-8.

[17] S. Wang, J. Hu, and X. Yuan, "Virtual synchronous control for grid-connected DFIG-based wind turbines," *IEEE Journal of Emerging and Selected Topics in Power Electronics*, vol. 3, no. 4, pp. 932-944, Dec. 2015.

[18] L. Shang, J. Hu, X. Yuan *et al*., "Improved virtual synchronous control for grid-connected VSCs under grid voltage unbalanced conditions," *Journal of Modern Power Systems and Clean Energy*, vol. 7, no. 1, pp. 174-185, Jan. 2019.

[19] J. Xi, H. Geng, S. Ma *et al*., "Inertial response characteristics analysis and optimisation of PMSG-based VSG-controlled WECS," *IET Renewable Power Generation*, vol. 12, no. 15, pp. 1741-1747, Nov. 2018.

[20] L. Chang-Chien, W. Lin, and Y. Yin, "Enhancing frequency response control by DFIGs in the high wind penetrated power systems," *IEEE Transactions on Power Systems*, vol. 26, no. 2, pp. 710-718, May 2011.

[21] F. Gao and M. R. Iravani, "A control strategy for a distributed generation unit in grid-connected and autonomous modes of operation," *IEEE Transactions on Power Delivery*, vol. 23, no. 2, pp. 850-859, Apr. 2008.

[22] S. Tan , H. Geng , G. Yang *et al*., "Modeling framework of voltage-source converters based on equivalence with synchronous generator," *Journal of Modern Power Systems and Clean Energy*, vol. 6, no. 6, pp. 1291-1305, Nov. 2018.

[23] Z. Wu , W. Gao, T. Gao *et al*., "State-of-the-art review on frequency response of wind power plants in power systems," *Journal of Modern Power Systems and Clean Energy*, vol. 6, no. 1, pp. 1-16, Jan. 2018.

[24] S. Li, T. A. Haskew, and L. Xu, "Conventional and novel control designs for direct driven PMSG wind turbines," *Electric Power System Research*, vol. 8, no. 3, pp. 328-338, Mar. 2010.

[25] J. F. Conroy and R. Watson, "Frequency response capability of full converter wind turbine generators in comparison to conventional generation," *IEEE Transactions on Power Systems*, vol. 23, no. 2, pp. 649-656, May 2008.

[26] S. Bayhan, H. Fidanboy, and S. Demirbas, "Active and reactive power control of grid connected permanent magnet synchronous generator in wind power conversion system," in *Proceedings of 2013 International Conference on Renewable Energy Research and Applications*, Madrid, Spain, Oct. 2013, pp. 1048-1052.

[27] H. Geng, G. Yang, D. Xu *et al*., "Unified power control for PMSG-based WECS operating under different grid conditions," *IEEE Transactions on Energy Conversion*, vol. 26, no. 3, pp. 822-830, Sept. 2011.

[28] P. Kundur, *Power System Stability and Control*. New York: McGraw-Hill, 1994.

[29] S. A. M. Saleh, "Testing the performance of a resolution-level MPPT controller for PMG-based wind energy conversion systems," *IEEE Transactions on Industry Applications*, vol. 53, no. 3, pp. 2526-2540, May 2017.

[30] Z. M. Dalala, Z. U. Zahid, and J. S. Lai, "New overall control strategy for small-scale WECS in MPPT and stall regions with mode transfer control," *IEEE Transactions on Energy Conversion*, vol. 28, no. 4, pp. 1082-1092, Dec. 2013.

[31] N. A. Janssens, G. Lambin, and N. Bragard, "Active power control strategies of DFIG wind turbines," in *Proceedings of IEEE Lausanne PowerTech*, Lausanne, Switzerland, Jul. 2007, pp. 516-521.

Jiangbei Xi received the B.S. degree in control science and control engineering from Huazhong University of Science and Technology, Wuhan, China, in 2012, and the M.S. degree in power electronics from Zhejiang University, Hangzhou, China, in 2015. He is currently working toward the Ph.D. degree in Tsinghua University, Beijing, China. His research interest includes control science and engineering.

Hua Geng received the B.S. degree in electrical engineering from Huazhong University of Science and Technology, Wuhan, China, in 2003, and the Ph.D. degree in control theory and application from Tsinghua University, Beijing, China, in 2008. From 2008 to 2010, he was a Postdoctoral Research Fellow with the Department of Electrical and Computer Engineering, Ryerson University, Toronto, Canada. He currently is an Associate Professor of Tsinghua University. His current research interests include advanced control on power electronics and renewable energy conversion systems.

Xin Zou received the B.S. degree in electrical engineering from North China Electric Power University, Baoding, China, in 2003, and the Ph.D. degree in electrical engineering from Tsinghua University, Beijing, China, in 2011. She joined the State Grid Economic and Technological Research Institute Co. Ltd, Beijing, China, in 2012, and currently is a Deputy Director in the transmission power grid planning division. She is a Senior Engineer of electrical engineering and technology, a Certified Consulting Engineer and a Certified Plant Engineering Consultant. Her currently research interests include power system planning, DC transmission system designing, and power system analysis.